

# Characterization of modified $\alpha$ -LiNbWO<sub>6</sub> layered materials and their catalytic performance for toluene nitration

YUAN WANG<sup>a,b</sup>, RUI DONG<sup>b</sup>, AN LI<sup>a</sup>, LIFANG HU<sup>a</sup>, JIE HE<sup>\*a</sup>

<sup>a</sup>School of Chemical Engineering, Anhui University of Science and Technology, Huainan, 232001 P. R. China

<sup>b</sup>Chemical and Biological Engineering College, Yancheng Institute of Technology, Yancheng, 224051 P. R. China

Layered material  $\alpha$ -LiNbWO<sub>6</sub> was prepared by solid-state method, HNbWO<sub>6</sub>, Fe<sub>1/3</sub>NbWO<sub>6</sub> and HNbWO<sub>6</sub>/Fe<sub>2</sub>O<sub>3</sub>-SO<sub>4</sub><sup>2-</sup> were prepared by the methods such as ion-exchange, intercalation and impregnation based on the parent material. The phase structures, morphologies, skeleton characteristics and acidic properties of the materials were characterized by powder X-ray diffraction (XRD), scanning electron microscope (SEM), fourier transform infrared spectroscopy (FT-IR) and NH<sub>3</sub> temperature-programmed desorption (NH<sub>3</sub>-TPD). Results show that the gallery height of the materials vary with the difference interlayer species and the acid strength follows the order HNbWO<sub>6</sub>/Fe<sub>2</sub>O<sub>3</sub>-SO<sub>4</sub><sup>2-</sup> > HNbWO<sub>6</sub> > Fe<sub>1/3</sub>NbWO<sub>6</sub>. HNbWO<sub>6</sub>/Fe<sub>2</sub>O<sub>3</sub>-SO<sub>4</sub><sup>2-</sup> shows the best catalytic activity and the highest selectivity for toluene nitration.

(Received September 22, 2014; accepted February 10, 2016)

**Keywords:** Modified  $\alpha$ -LiNbWO<sub>6</sub>, Phase structures, Acidic properties, Toluene nitration, Regioselective

## 1. Introduction

*Para*-mononitrotoluene (*p*-MNT) is an important intermediate in the formation of many industrial products, such as pharmaceuticals, dyes, pesticides and plastics. In the traditional industrialized production, *p*-MNT is synthesised by liquid phase toluene nitration using HNO<sub>3</sub> as the nitrating reagent and H<sub>2</sub>SO<sub>4</sub> as the catalyst, which called mixed acid nitration system [1,2]. However, the classic system has some disadvantages, such as equipment corrosion, over-nitration, waste acid treatment, etc [3]. The typical products distribution of *ortho*-, *meta*- and *para*-isomer in the traditional nitration process is about 58:4:38 [4], that is to say the percent of *p*-MNT is relatively low. Therefore, new catalysts and novel nitration technologies are urgently needed to overcome such problems.

In order to increase the ratio of *para*- to *ortho*- (*p/o*) and overcome the drawback of the mixture acid nitration system, some solid acid catalysts have been investigated for toluene nitration in the liquid or vapor phase. R. J. Kalbasi [5] used H<sub>3</sub>PO<sub>4</sub>/ZSM-5 zeolite that modified by N-cetylpyridinium bromide as the catalysts for vapor phase toluene nitration, the results showed that a higher *para*-selectivity was obtained over the modified catalyst because the major part of the reaction was carrying out in the pores of zeolites. S. S. Kim [6] used H<sup>+</sup>-ZSM-5 and NH<sub>4</sub><sup>+</sup>-ZSM-5 as catalysts, they also proved that the shape-selective micropores of the molecular sieve catalysts

was existed in toluene nitration. M. G. Kuba [7] used zeolites beta to catalyze the vapor phase toluene nitration and the *para*-selectivity also can be improved. Other catalysts, such as solid superacids SO<sub>4</sub><sup>2-</sup>/TiO<sub>2</sub>-CeO<sub>2</sub> [8], SO<sub>4</sub><sup>2-</sup>/ZrO<sub>2</sub>-TNTs [9] and supported heteropoly acid H<sub>3</sub>PW<sub>12</sub>O<sub>40</sub>/SiO<sub>2</sub> [10], have also been used for toluene nitration, they can improved the *para*-selectivity or the conversion rate of toluene to some extent. These researchs suggest that the acid strength and the shape selectivity of catalysts are very important to obtain higher conversion rate and *para*-selectivity for toluene nitration.

The layered niobium-based composite oxides are becoming more and more attractive materials due to their thermal stability and strong acidity [11-14]. Just like zeolites, their layer spacing can be modified to achieve the shape-selective purposes for transition state and the product. As an important protonated layered material, HNbWO<sub>6</sub> has been studied due to its exceptional catalytic activity and the exchangeable property of the interlayer cations [15-17]. A. Takagaki et al. [18] used modified HNbWO<sub>6</sub> as the catalyst for Friedel-Crafts alkylation and it showed a significant catalytic activity. X. J. Guo and co-workers [19] studied the synthesis and properties of CrO<sub>x</sub>-pillared HNbWO<sub>6</sub>, the result indicated that the materials had a potential application as the efficient catalyst for photodegradation of some organic compounds.

In the present study, the layered materials HNbWO<sub>6</sub>, Fe<sub>1/3</sub>NbWO<sub>6</sub> and HNbWO<sub>6</sub>/Fe<sub>2</sub>O<sub>3</sub>-SO<sub>4</sub><sup>2-</sup> are prepared, their phase structures, morphologies, skeleton characteristics

and acidic properties are characterized by XRD, SEM, FT-IR and NH<sub>3</sub>-TPD. Their catalytic activities are evaluated using the nitration of toluene in a batch reactor.

## 2. Experimental

### 2.1 Preparation of the layered materials

HNbWO<sub>6</sub> and Fe<sub>1/3</sub>NbWO<sub>6</sub> were prepared by ion-exchange reaction of  $\alpha$ -LiNbWO<sub>6</sub> with 2 mol·dm<sup>-3</sup> HNO<sub>3</sub> or Fe(NO<sub>3</sub>)<sub>3</sub> aqueous solution at 333 K for 96 h, the solution was replaced with a fresh every 24 h during the period. The products were washed with distilled water and dried in air at 333 K for 12 h. The parent  $\alpha$ -LiNbWO<sub>6</sub> was prepared by calcining the mixture of the stoichiometric Li<sub>2</sub>CO<sub>3</sub>, Nb<sub>2</sub>O<sub>5</sub> and WO<sub>3</sub> at 1033 K for 72 h, the detailed process have been reported in our earlier work [20].

HNbWO<sub>6</sub>/Fe<sub>2</sub>O<sub>3</sub> was prepared through intercalating Fe<sub>2</sub>O<sub>3</sub> into the interlayer of HNbWO<sub>6</sub>. The procedure is as follows [17]: Firstly, HNbWO<sub>6</sub>/n-C<sub>3</sub>H<sub>7</sub>NH<sub>2</sub> was prepared by reaction of 4 g HNbWO<sub>6</sub> and 200 ml 20%vol n-C<sub>3</sub>H<sub>7</sub>NH<sub>2</sub>/n-hexane mixture at 323 K for 72 h, after filtered and washed with ethanol absolute and distilled water, the powder dried for 24 h at 353 K. Secondly, 2 g HNbWO<sub>6</sub>/n-C<sub>3</sub>H<sub>7</sub>NH<sub>2</sub> reacted with 22 g [Fe<sub>3</sub>(CH<sub>3</sub>COO)<sub>7</sub>(OH)(H<sub>2</sub>O)<sub>2</sub>]NO<sub>3</sub> in 100 ml water at 323 K for 72 h, the solid product was washed and dried at 353 K for 12 h. Lastly, the powder was calcined at 573 K for 3 h.

HNbWO<sub>6</sub>/Fe<sub>2</sub>O<sub>3</sub>-SO<sub>4</sub><sup>2-</sup> was obtained by impregnation method, 1 g HNbWO<sub>6</sub>/Fe<sub>2</sub>O<sub>3</sub> added into 15 ml 0.4 mol·dm<sup>-3</sup> (NH<sub>4</sub>)<sub>2</sub>SO<sub>4</sub> at room temperature, string for 24 h. The powder was washed, dried and calcined at 573 K for 3 h.

### 2.2 Characterization

Powder X-ray diffraction (XRD) patterns were collected on a powder diffractometer XD-3 (Beijing Purkinje General Instrument Co., Ltd.) with a curved graphite-monochromatied CuK $\alpha$  radiation ( $\lambda = 1.5406 \text{ \AA}$ ) operating at 40 kV and 30 mA. SEM images of the samples were obtained by a Quanta 200 scanning electron microscope (SEM) with an acceleration voltage of 20 kV. Fourier-transform Infrared (FT-IR) spectra of the materials dispersed in KBr were recorded on a Bruker Vector 33 spectrophotometer (DTGS detector).

NH<sub>3</sub>-TPD experiments were carried out in a continuous flow fixed-bed reactor system with thermal conduction detector (TCD) (Tianjin xianquan, industry & trade development Co., Ltd.). In TPD measurements, 100 mg of the sample was placed in a quartz tube and heated at

453 K in a flow of He (30 ml·min<sup>-1</sup>, 99.99 %) for 1 h, exposed to NH<sub>3</sub> at 333 K for adsorption until it was saturated, removed of the excess NH<sub>3</sub> by exposing the sample at 333 K for 1 h, and finally heated at 10 K·min<sup>-1</sup>.

### 2.3 Acid-Catalyzed experiment

The catalytic activity of the materials was evaluated by nitration of toluene. The reaction was performed in a 100 ml three-necked flask in batch. 5.0 ml toluene, 15 ml CCl<sub>4</sub>, 6.0 ml acetic acid anhydride and a certain amount of catalyst, 5.0 ml 95 wt% nitric acid were added in sequence to the flask. The reaction was run for 2.5 h at 313K. The organic phase was separated, and washed with 5 wt% NaHCO<sub>3</sub> solution and deionized water. The products were quantitative analyzed by GC with hydrogen flame ionization detector (FID) using a PEG-20M column.

## 3. Results and discussion

### 3.1 Phase structure and morphology of the materials

The XRD patterns of the materials are presented in Fig. 2. The pattern of the parent  $\alpha$ -LiNbWO<sub>6</sub> (Fig. 1a) matches well with JCPDS 41-0378. It is quite clear that  $\alpha$ -LiNbWO<sub>6</sub> has a three dimensional layered structure based on the diffraction peaks at  $2\theta = 9.51^\circ$ ,  $19.12^\circ$  and  $26.87^\circ$ . The parent  $\alpha$ -LiNbWO<sub>6</sub> that belongs to tetragonal crystal system, has a main plane of (001) and the unit cell parameter  $c = 0.928 \text{ nm}$ . After exchange by H<sup>+</sup> or Fe<sup>3+</sup>, the main plane shifts to (002) from (001). At the same time, the corresponding crystal cell parameter  $c$  changes to 2.590 or 2.560 nm, respectively. It could be because that the adjacent slabs of the parent  $\alpha$ -LiNbWO<sub>6</sub> occurs a relative sliding and forms a continuous “groove” and “convex column” (Fig. 2) in condition of maintaining the original unit cell during the process of ion-exchange [21].

The diffraction peaks corresponding to (002) plane of HNbWO<sub>6</sub>/Fe<sub>2</sub>O<sub>3</sub> and HNbWO<sub>6</sub>/Fe<sub>2</sub>O<sub>3</sub>-SO<sub>4</sub><sup>2-</sup> shift to  $8.02^\circ$  and  $7.76^\circ$ , and they remain the same main plane as corresponding that of HNbWO<sub>6</sub>. Similarly, the corresponding crystal cell parameters  $c$  are 2.204 and 2.278 nm, respectively. It is noted that several diffraction peaks (marked as ☆) can be observed in the Fig. 1 d and e, which can be easily indexed to hexagonal  $\alpha$ -Fe<sub>2</sub>O<sub>3</sub> (JCPDS 33-0664). The results mean that  $\alpha$ -Fe<sub>2</sub>O<sub>3</sub> can be inserted into the interlayer successfully.

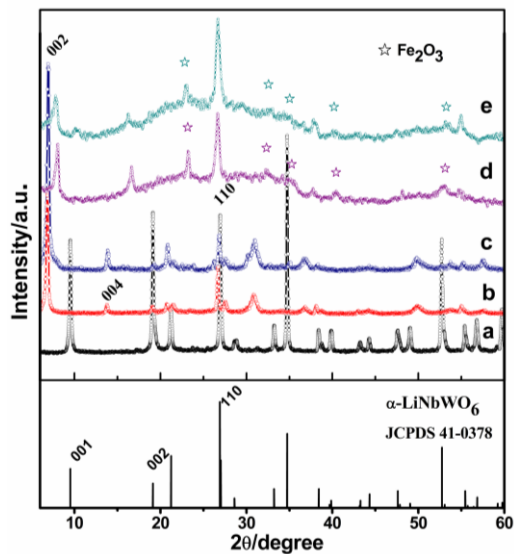


Fig. 1. XRD patterns of the materials  
 a.  $\alpha$ -LiNbWO<sub>6</sub>; b. HNbWO<sub>6</sub>; c. Fe<sub>1/3</sub>NbWO<sub>6</sub>;  
 d. HNbWO<sub>6</sub>/Fe<sub>2</sub>O<sub>3</sub>; e. HNbWO<sub>6</sub>/Fe<sub>2</sub>O<sub>3</sub>-SO<sub>4</sub><sup>2-</sup>

The  $d$ -spacing values along their main plane are calculated based on the Bragg equation  $\lambda=2d\sin\theta$ . According to the calculation method which we mentioned before [20], the gallery height of HNbWO<sub>6</sub>, Fe<sub>1/3</sub>NbWO<sub>6</sub>, HNbWO<sub>6</sub>/Fe<sub>2</sub>O<sub>3</sub>-SO<sub>4</sub><sup>2-</sup> are 0.518, 0.503 and 0.362 nm, respectively. For HNbWO<sub>6</sub> and Fe<sub>1/3</sub>NbWO<sub>6</sub>, the corresponding  $d$ -spacing increases to 1.295 and 1.280 nm, respectively. It is because H<sup>+</sup> and Fe<sup>3+</sup> are prone to hydration and they exist in the form of hydrated H<sup>+</sup> and hydrated Fe<sup>3+</sup> between the layers. The gallery height of HNbWO<sub>6</sub>/Fe<sub>2</sub>O<sub>3</sub> is 0.324 nm, the result is basically consistent with the reported in literature [17]. However, the gallery height is increased slightly after impregnation by (NH<sub>4</sub>)<sub>2</sub>SO<sub>4</sub>.

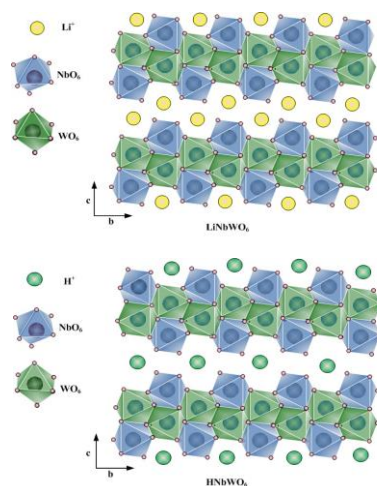


Fig. 2. Schematic structures of layered materials

SEM images are shown in Fig. 3. The image (Fig. 3a) shows that the parent  $\alpha$ -LiNbWO<sub>6</sub> exhibits a plate-like morphology. After ion-exchange, the modified materials almost remain the regular layered structure, which have been confirmed by the XRD technology. However, the images of Fe<sub>2</sub>O<sub>3</sub>/HNbWO<sub>6</sub> and Fe<sub>2</sub>O<sub>3</sub>/HNbWO<sub>6</sub>-SO<sub>4</sub><sup>2-</sup> present the fluffy and irregular morphology, they may be mainly attributed to the dehydroxylation and dehydration of the Fe<sub>2</sub>O<sub>3</sub> guest nanoparticles to oxide pillars during the calcination process.

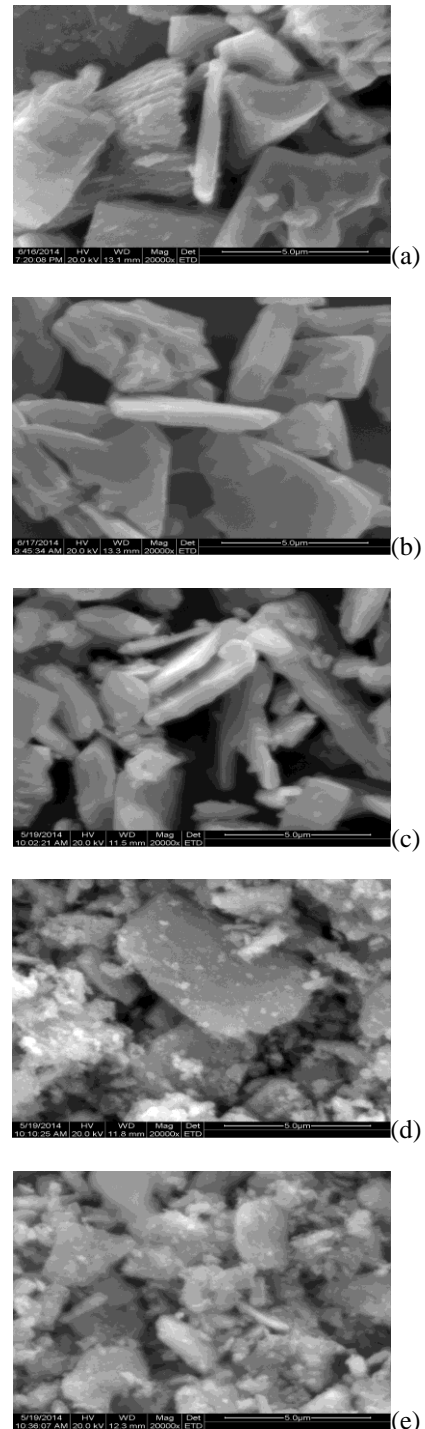


Fig. 3. SEM images of (a) $\alpha$ -LiNbWO<sub>6</sub>; (b)HNbWO<sub>6</sub>  
 (c)Fe<sub>1/3</sub>NbWO<sub>6</sub>; (d)HNbWO<sub>6</sub>/Fe<sub>2</sub>O<sub>3</sub>; (e)HNbWO<sub>6</sub>/Fe<sub>2</sub>O<sub>3</sub>-SO<sub>4</sub><sup>2-</sup>

### 3.2 Skeleton characteristics of the materials

Fig. 4 shows the FT-IR spectra of the materials, the band position and their attribution are summarized in Table 1 based on the references [20, 22-28].

When the interlayer Li<sup>+</sup> in  $\alpha$ -LiNbWO<sub>6</sub> is exchanged by H<sup>+</sup> or Fe<sup>3+</sup> ion, the Nb=O band is shifted from 881.6 cm<sup>-1</sup> to higher wavenumbers of 910.1 and 910.3 cm<sup>-1</sup>, the W=O is shifted to 982.6 and 982.2 cm<sup>-1</sup>, respectively. The vibration of the O–M–O (M = Nb, W) bonds are also affected by the interlayer cations.

HNbWO<sub>6</sub>/Fe<sub>2</sub>O<sub>3</sub> is just an intermediate. Therefore, focus is placed on the differences of the FT-IR spectra between HNbWO<sub>6</sub>/Fe<sub>2</sub>O<sub>3</sub>-SO<sub>4</sub><sup>2-</sup> and HNbWO<sub>6</sub>. Compared with HNbWO<sub>6</sub>, one can find that the band corresponding to the vibration of W=O has a blue shift, and the bands corresponding to the vibration of O–W–O and the antisymmetric stretching vibration of O–Nb–O are red shifted. The results suggest that those terminal and bridge bonds are influenced by intercalation oxide. The bands located at approximately 530.6 cm<sup>-1</sup> can be attributed to the vibration of Fe–O. In addition, there is an absorption band around 657.9 cm<sup>-1</sup>, which can be assigned to asymmetric vibration of S–O [26]. Four obvious absorption bands which are located at 1078.3, 1137.5,

1222.2 and 1271.0 cm<sup>-1</sup> can be also observed, they are the characteristic bands of a bidentate SO<sub>4</sub><sup>2-</sup> coordinated to the metal Fe<sub>2</sub>O<sub>3</sub> [27-28]. Then we can deduce that intercalation oxide Fe<sub>2</sub>O<sub>3</sub> has reacted with (NH<sub>4</sub>)<sub>2</sub>SO<sub>4</sub> and formed sulfate. It is the basis that HNbWO<sub>6</sub>/Fe<sub>2</sub>O<sub>3</sub>-SO<sub>4</sub><sup>2-</sup> material has a property of the super acid.

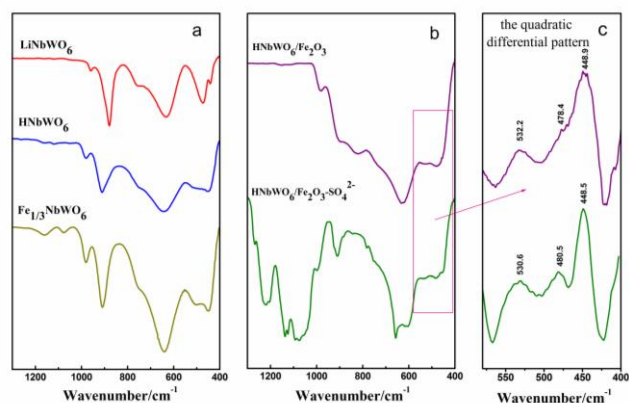


Fig. 4. FT-IR pattern of the materials

Table 1. Infrared band assignments of the materials

|   | LiNbWO <sub>6</sub> | HNbWO <sub>6</sub> | Fe <sub>1/3</sub> NbWO <sub>6</sub> | HNbWO <sub>6</sub><br>/ Fe <sub>2</sub> O <sub>3</sub> | HNbWO <sub>6</sub><br>/Fe <sub>2</sub> O <sub>3</sub> -SO <sub>4</sub> <sup>2-</sup> | References |
|---|---------------------|--------------------|-------------------------------------|--|--|------------|
| $\nu_s(\text{Nb}=\text{O})$                                 | 881.6               | 910.1              | 910.3                               | 905.8  | 913.2  | [23]       |
| $\nu_s(\text{W}=\text{O})$                                  | 960.3               | 982.6              | 982.2                               | 980.2  | 995.0  | [22]       |
| $\nu_{as}(\text{O}-\text{Nb}-\text{O})$                     | 474.4               | 514.0              | 505.4                               | 478.4  | 480.5  | [24]       |
| $\nu_s(\text{O}-\text{Nb}-\text{O})$                        | 439.0               | 449.7              | 449.6                               | 448.9  | 448.5  | [24]       |
| $\nu_s(\text{O}-\text{W}-\text{O})$                         | 632.4               | 640.5              | 642.4                               | 628.7  | 615.7  | [22]       |
| $\nu_s(\text{W}-\text{O}-\text{Nb})$                        | 758.3               | 758.3              | 755.2                               | 743.2  | 755.8  | [20]       |
| $\nu(\text{Fe}-\text{O})$                                   |                     |                    |                                     | 532.2  | 530.6  | [25]       |
| $\nu(\text{S}-\text{O})$                                    |                     |                    |                                     |  | 657.9  | [26]       |
|   |                     |                    |                                     |  | 1078.3   | [28]       |
| SO <sub>4</sub> <sup>2-</sup> $\nu_{as}(\text{S}=\text{O})$ |                     |                    |                                     |  | 1222.2   | [28]       |
|   |                     |                    |                                     |  | 1137.5   | [10]       |
| $\nu_s(\text{S}=\text{O})$                                  |                     |                    |                                     |  | 1271.0   | [27]       |

### 3.3 The acidic properties of the materials

NH<sub>3</sub>-TPD is one of the basic methods to measure the acidic properties of catalytic materials, and the NH<sub>3</sub>-TPD profiles of the materials are shown in Fig. 5. Their total acid amounts are calculated and the results are shown in Table 2.

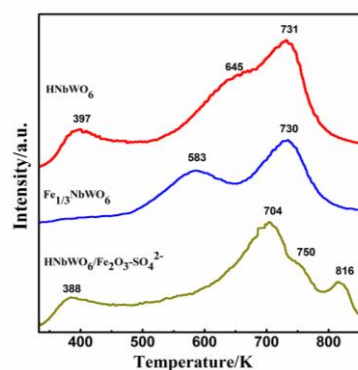


Fig. 5. NH<sub>3</sub>-TPD profiles of the materials

Table 2. The desorption peak position and the total acid amount of the materials

| Catalysts   | Peak position /K   | Acid amount /(mmol/g) |
|---|--------------------|-----------------------|
| HNbWO <sub>6</sub>  | 397 645 731        | 0.68                  |
| Fe <sub>1/3</sub> NbWO <sub>6</sub>   | 583 730            | 0.31                  |
| HNbWO <sub>6</sub> /Fe <sub>2</sub> O <sub>3</sub> -SO <sub>4</sub> <sup>2-</sup> | 388 704<br>750 816 | 0.48                  |

As shown in Table 2, HNbWO<sub>6</sub>/Fe<sub>2</sub>O<sub>3</sub>-SO<sub>4</sub><sup>2-</sup> has desorption peaks at 750 and 816 K, which corresponding to the strong acid sites. HNbWO<sub>6</sub> and Fe<sub>1/3</sub>NbWO<sub>6</sub> have almost the same strong acid sites, the desorption peak is located at about 730 K. Compared to HNbWO<sub>6</sub>, the acid strength and acid amount of Fe<sub>1/3</sub>NbWO<sub>6</sub> has decreased due to different ions between the layers. Table 2 also shows that HNbWO<sub>6</sub>/Fe<sub>2</sub>O<sub>3</sub>-SO<sub>4</sub><sup>2-</sup> has the strongest acid strength, and HNbWO<sub>6</sub> has the biggest acid amount which is twice more than that of Fe<sub>1/3</sub>NbWO<sub>6</sub>.

We know that the layered oxide which is as a solid acid catalyst usually contain at least one of Lewis acid (L acid) sites and Brønsted acid (B acid) sites [20]. L acid sites come from central metal ions of MO<sub>6</sub> octahedral structure unit of the layered compounds, B acid sites come from interlayer H<sup>+</sup> ions or the protonated hydroxyl groups. For HNbWO<sub>6</sub> and HNbWO<sub>6</sub>/Fe<sub>2</sub>O<sub>3</sub>-SO<sub>4</sub><sup>2-</sup>, the sites is mainly consisted of the B acid sites. The B acid sites, especially the strong B acid sites, are important for nitration of toluene.

### 3.4 Acid catalytic activity

In present toluene nitration system, acetic anhydride has been proved that it not only can make the reaction more moderate in activity but also can remove the water that generated during the reaction. In addition, the presence of acetic anhydride can provide high selectivity for the para-isomer product [29-31].

The catalytic performance of HNbWO<sub>6</sub>, Fe<sub>1/3</sub>NbWO<sub>6</sub> and HNbWO<sub>6</sub>/Fe<sub>2</sub>O<sub>3</sub>-SO<sub>4</sub><sup>2-</sup> for the toluene nitration is shown in Fig. 6. The ratio of *p/o* over the three catalysts is 1.02, 1.01, and 1.20, respectively. In the absence of catalyst, the value of *p/o* is 0.77 and the conversion rate is 58.9%, which could be attributed to the self-catalysis effect of fuming nitric acid and the ability of the acetic anhydride to remove water during the nitration. Furthermore, the conversion rate of toluene can reach more than 90.0% in the current conditions over the materials.

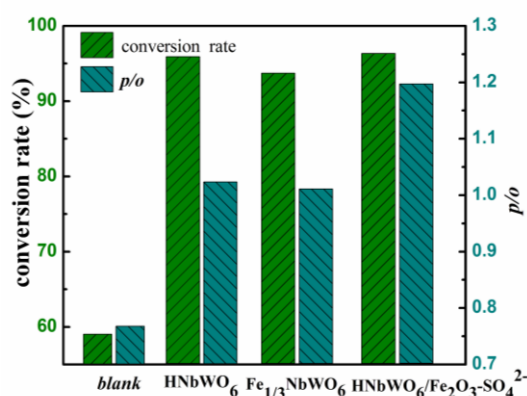


Fig. 6. Catalytic activities for toluene nitration by the materials

Based on the Ingold-Hughes mechanism for electrophilic aromatic nitration theory [2, 32], and the special structure of the materials, toluene nitration process using HNbWO<sub>6</sub> as the catalyst are conjectured as shown in Fig. 7. First, nitric acid entered into the interlayer of HNbWO<sub>6</sub> which then reacted with the interlayer H<sup>+</sup>, one molecule water and nitronium ion (NO<sub>2</sub><sup>+</sup>) generated at the same time. Lastly, NO<sub>2</sub><sup>+</sup> reacted with toluene to generate nitrotoluene. It has been known that the gallery height of the HNbWO<sub>6</sub> is 0.518 nm and the kinetic diameter of toluene is about 0.525 nm. Since the presence of NO<sub>2</sub><sup>+</sup> in the interlayer, the gallery height might have become easier for toluene molecules to penetrate into the interlayer. What is more, for the three possible mononitration isomers of toluene, only the kinetic diameter of *p*-MNT can easily diffuse out from the interlayer of HNbWO<sub>6</sub> [33]. Thus, the ratio of *p/o* in the toluene nitration over HNbWO<sub>6</sub> catalyst is significantly higher than that of without catalyst. Fe<sub>1/3</sub>NbWO<sub>6</sub> and HNbWO<sub>6</sub> have almost the same catalytic selectivity due to their close gallery height and acid strength. HNbWO<sub>6</sub>/Fe<sub>2</sub>O<sub>3</sub>-SO<sub>4</sub><sup>2-</sup> has a gallery height of 0.356 nm, which is smaller than the kinetic diameter of toluene. As a result, toluene diffusion into the interlayer of the HNbWO<sub>6</sub>/Fe<sub>2</sub>O<sub>3</sub>-SO<sub>4</sub><sup>2-</sup> is difficult.

However, HNbWO<sub>6</sub>/Fe<sub>2</sub>O<sub>3</sub>-SO<sub>4</sub><sup>2-</sup> shows the best catalytic activity among the three catalysts for the toluene nitration. According to the Ingold-Hughes mechanism, the nitration reaction yield and selectivity could be enhanced in the environment of strong acid [34]. So it still can obtain higher ratio of *p/o* when it used as catalyst because of its stronger acid sites. Combining with the result shown in Fig. 5 and Fig. 6, it can be clearly see that there is little relationship between the catalytic activity of nitration and the acid amount of the weak sites for these catalysts. These results indicate that the acid strength and the gallery height are the important factors to affect the catalytic activity and selectively in the toluene nitration.

According to our calculation based on the XRD results, the gallery height of the HNbWO<sub>6</sub>/Fe<sub>2</sub>O<sub>3</sub>-SO<sub>4</sub><sup>2-</sup> is still not enough for toluene shape-selective nitration. Thus,

the ratio of  $p/o$  is not enough high compared to the molecular sieve catalyst, although it is increased due to the presence of strong acid sites. Consequently, future work about using this catalyst system (modified  $\alpha$ -LiNbWO<sub>6</sub>) to increase the para-selectivity of toluene nitration would be further studied.

#### 4. Conclusion

For the layered materials HNbWO<sub>6</sub>, Fe<sub>1/3</sub>NbWO<sub>6</sub> and HNbWO<sub>6</sub>/Fe<sub>2</sub>O<sub>3</sub>-SO<sub>4</sub><sup>2-</sup>, the interlayer species dramatically affect the interlayer spacing, also affect the acid amount and the acid strength. HNbWO<sub>6</sub> has the largest gallery height and the HNbWO<sub>6</sub>/Fe<sub>2</sub>O<sub>3</sub>-SO<sub>4</sub><sup>2-</sup> shows the obvious characteristics of strong acid. For the materials, their catalytic activities for toluene nitration are affected by both the gallery height and the acid strength. The strong acid sites is the main catalytic active site in this reaction. The interlayer superacid sites and the enough gallery height will help to improve the ratio of  $p/o$  in the process of the toluene nitration for the protonated layered composite materials.

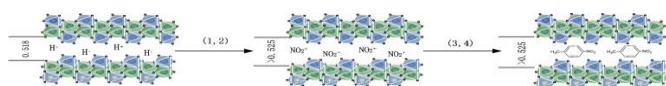


Fig. 7. The schematic diagram of the toluene nitration process

#### Acknowledgments

This work was supported by the Natural Science Foundation of China (No. 21071004), Anhui Provincial Natural Science Foundation (No. 11040606M38) and Research Fund of Key Laboratory for Advanced Technology in Environmental Protection of Jiangsu Province (AE201106).

#### References

- [1] J. M. Zaldiva, E. Molga, M. A. Alós, H. Hernández, K. R. Westerterp, *Chem. Eng. Process.* **35**, 91 (1996).
- [2] I. Sreedhar, M. Singha, K. V. Raghavan, *Catal. Sci. Technol.* **3**, 2499 (2013).
- [3] Y. H. Zhao, F. J. Jiao, G. W. Chen, Q. Yuan, *AIChE J.* **57**, 1409 (2011).
- [4] P. D. Sharda, B. W. Suresh, S. K. Vijay, K. D. Mohan, *Appl. Catal. A: Gen.* **226**, 49 (2002).
- [5] R. J. Kalbasi, M. Ghiaci, A. R. Massah, *Appl. Catal. A: Gen.* **353**, 1 (2009).
- [6] S. S. Kim, J. P. Thomas, *J. Catal.* **253**, 289 (2008).
- [7] M. G. Kuba, R. Prins, G. D. Pirngruber, *Appl. Catal. A: Gen.* **333**, 78 (2007).
- [8] W. Mao, H. Z. Ma, B. Wang, *J. Hazard. Mater.* **167**, 707 (2009).
- [9] P. F. Chen, M. X. Du, H. Lei, Y. Wang, G. L. Zhang, F. B. Zhang, *Catal. Commun.* **18**, 4 (2012).
- [10] X. Q. Zhao, Y. T. Han, X. L. Sun, Y. J. Wang, *Chin. J. Catal.* **28**, 91 (2007).
- [11] C. Tagusagawa, A. Takagaki, S. Hayashi, K. Domen, *Catal. Today*, **142**, 267 (2009).
- [12] W. M. Cai, G. H. Lu, J. He, Y. X. Lan, *Ceram. Int.* **38**, 3167 (2012).
- [13] X. R. Fan, B. Zh. Lin, H. Liu, L. W. He, Y. L. Chen, B. F. Gao, *Int. J. Hydrogen Energy.* **38**, 832 (2013).
- [14] N. N. Wang, Y. X. Lan, J. He, R. Dong, J. S. Hu, *Bull. Korean. Chem. Soc.* **34**, 2737 (2013).
- [15] G. K. Prasad, T. Takei, K. Arimoto, Y. Yonesaki, N. Kumada, N. Kinomura, *Solid State Ionics.* **177**, 197 (2006).
- [16] T. N. Sairam, B. J. Viswanathan, *Phys. Chem. Solids.* **63**, 317 (2002).
- [17] J. H. Wu, S. Uchida, Y. Fujishiro, Sh. Yin, T. Sato, *J. Photoch. Photobio. A.* **128**, 129 (1999).
- [18] A. Takagaki, C. Tagusagawa, S. Hayashi, *Energy Environ. Sci.* **3**, 82 (2010).
- [19] X. J. Guo, S. F. Wang, S. M. Liu, L. Zhao, T. Yu, W. F. Duan, X. Q. Xu, *Inorg. Chim. Acta.* **421**, 307 (2014).
- [20] J. He, Q. J. Li, Y. Tang, P. Yang, A. Li, R. Li, H. Z. Li, *Appl. Catal. A: Gen.* **443-444**, 145 (2012).
- [21] V. Bhat, J. Gopalakrishnan, *Solid State Ionics.* **26**, 25 (1988).
- [22] J. Cao, B. D. Luo, H. L. Lin, B. Y. Xu, Sh. F. Chen, *Appl. Catal. B: Environ.* **111**, 288 (2012).
- [23] Y. J. Lu, R. Lalancette, H. B. Robert, *Inorg. Chem.* **35**, 2524 (1996).
- [24] C. C. Owen, E. O. Frank, *J. Phys. Chem. C.* **113**, 479 (2009).
- [25] M. Žic, M. Ristić, S. Musić, *J. Mol. Struct.* **993**, 115 (2011).
- [26] S. Musić, A. Šarić, S. Popović, T. Sawada, *Croat. Chem. Acta.* **73**, 541 (2000).
- [27] H. F. Guo, P. Yan, X. Y. Hao, Zh. Zh. Wang, *Mater. Chem. Phys.* **112**, 1065 (2008).
- [28] K. R. Sunaja-Devi, S. Jayashree, *Bull. Chem. React. Eng. Cataly.* **7**, 205 (2013).
- [29] K. Smith, T. Gibbins, R. W. Millar, R. P. Claridge, *J. Chem. Soc.* **1**, 2753 (2000).
- [30] K. Smith, Mohammad Hayal Alotaibi, Gamal A. El-Hiti, *J. Catal.* **297**, 244 (2013).
- [31] S. Bernasconi, G. D. Pirngruber, A. Kogelbauer, R. Prins, *J. Catal.* **219**, 231 (2003).
- [32] P. M. Esteves, J. W. de, M. Carneiro, S. P. Cardoso, A. G. H. Barbosa, K. K. Laali, G. Rasul, G. K. S. Prakash, G. A. Olah, *J. Am. Chem. Soc.* **125**, 4836 (2003).
- [33] T. J. Kwok, K. Jayasuriya, *J. Org. Chem.* **59**, 4939 (1994).
- [34] O. Adamiak, D. Kalinowska-Alichnewicz, P. Maksimowski, W. Skupiński, *J. Mol. Catal. A-Chem.* **351**, 62 (2011).

\*Corresponding author: jhe@aust.edu.cn